Journal of Physics and Chemistry of Solids 84 (2015) 34–48

Contents lists available at ScienceDirect

Journal of Physics and Chemistry of Solids

journal homepage: www.elsevier.com/locate/jpcs

Review of superconductivity in BiS_2-based layered materials

Yoshikazu Mizuguchi *

Tokyo Metropolitan University, 1-1, Minami-osawa, Hachioji 192-0397, Japan

ARTICLE INFO

Article history:
Received 20 May 2014
Received in revised form
14 July 2014
Accepted 8 September 2014
Available online 18 September 2014

Keywords:
B. Chemical synthesis
B. Crystal growth
D. Superconductivity
D. Transport properties
D. Electronic structure

ABSTRACT

In 2012, a new layered superconductor where BiS_2 layer is the superconducting layer was discovered. So far, seven types of BiS_2-based superconductors and two related superconductors have been discovered. In this article, the diversity of the crystal structure and the physical properties of the BiS_2-based superconductors are reviewed. Furthermore, notable characteristics of superconductivity in the BiS_2 family are introduced. The prospects for raising T_c in this family are proposed on the basis of experimental and theoretical studies.

1. Introduction

In the field of new superconducting materials, breakthrough discoveries have focused layered materials in recent years. The most outstanding example is the Cu-oxide superconductors [1]. The layered Cu oxides which have CuO_2-type conductive layers were found to be superconductive with a transition temperature (T_c) higher than 77 K, the boiling point of liquid nitrogen [2,3]. Their characteristic crystal structure is an alternate stacking of the CuO_2 superconducting layers and blocking (insulating) layers. One of the most important facts is that many superconductors have been designed by changing the superconducting layers and/or the blocking layers. Among them, the highest recorded T_c is 135 K for the Hg-1223 superconductor at ambient pressure [4] and 153 K for the same material under a pressure of 15 GPa [5]. Furthermore, the discovery of the Cu-oxide superconductors resulted in rapid developments for applications on superconductivity.

In 2001, high-T_c superconductivity (T_c=39 K) was discovered in the binary compound MgB_2 [6]. The crystal structure of the MgB_2 superconductor is a layered structure like Cu-oxide superconductors. Due to the simple binary composition and low cost of the materials, MgB_2 is one of the promising materials for applications on superconductivity [7].

Another discovery of a high-T_c superconductor is accomplished in the layered materials with a Fe-square lattice (conductive layers) in 2008 [8]. As is the case with the Cu oxides, the crystal structure is composed of alternate stacks of the Fe-based superconducting layers and various types of blocking layers. The notable fact in the Fe-based family is that there are several types of superconducting layers such as Fe_2Pn_2 (Pn: P and As) or Fe_2Ch_2 (Ch: S, Se and Te) superconducting layers [8–17]. So far, the highest record of T_c is 58 K observed in $SmFeAsO_{1-x}F_x$ [9,18].

As introduced above, two kinds of "layered materials" have contributed to the development of high-T_c superconductors. There however are not the only layered superconductors which have provided us with some hints on how to understand the physics of unconventional superconductivity. In this regard, the discovery of new layered superconductors is one of the most important issues for the realization of a T_c approaching room temperature.

In 2012, we discovered novel layered superconductors which have a crystal structure similar to those of the Cu-oxide and Fe-based superconductors. The characteristic structure is an alternate stacking of superconducting BiS_2 layers and blocking layers. In the conduction plane, the Bi and S atoms are alternately aligned and form a Bi–S square plane. We call the new superconducting family "BiS_2-based superconductors" [19,20]. So far, 11 superconductors have been discovered in this family, and the highest record of T_c is 11 K in $LaO_{0.5}F_{0.5}BiS_2$ [21]. In addition, we should mention the Bi-oxide superconductor $B_{1-x}K_xBiO_3$ with a T_c of ~30 K [22,23]. The crystal structure is composed of an alternate stacking of $(Ba_{1-x}K_x)O$ planes and BiO_2 planes. In both BiS_2-based superconductors and $B_{1-x}K_xBiO_3$, Bi square planes with a relatively large Bi–Bi bonding play important roles for superconductivity. On the basis of these similarities of crystal structure and composing elements to the layered high-T_c superconductors, we consider that the T_c can be increased by optimizing the structure of superconducting layers and/or blocking layers in the BiS_2 family. In this article, the crystal structures and physical properties are summarized. Finally, the prospects for raising T_c in the BiS_2 family are discussed.

* Tel.: +81 42 677 2748; fax: +81 42 677 2756.
E-mail address: mizuguchi-yoshikazu@tmu.ac.jp

http://dx.doi.org/10.1016/j.jpcs.2014.09.003
0022-3697/

2. Crystal structure

The crystal structure of the BiS_2-based superconductors is basically composed of an alternate stacking of the double BiS_2 layers and the blocking layers. Fig. 1 shows a schematic of a typical BiS_2-based superconductor with three types of blocking layers. All the crystal structures are categorized into the tetragonal space group of *P4/nmm* or *I4/mmm*. The double BiS_2 conduction layers are categorized into a NaCl-type (rock-salt) structure. In the NaCl structure, cations (C) and anions (A) alternately occupy the sites of cubic lattice. When we take four C–A layers, we obtain a C_4A_4 layer structure. If the C sites of the first and fourth layers are removed, we obtain a C_2A_4 layer. The double BiS_2 layer (Bi_2S_4 layer) could be categorized into the C_2A_4-type layer.

Fig. 1(a) is a $REOBiS_2$-type structure whose blocking layer is REO (RE: La, Ce, Pr, Nd, Yb). In the $REOBiS_2$ type, conduction carriers can be controlled by partial substitutions at the O site by F (O/F substitution) [20,21,24–30] or the RE-site substitution by the M^{4+} ions (M: Th, Hf, Zr, Ti) [31]. When the REO blocking layers are replaced by SrF layers, we obtain $SrFBiS_2$-type structure (Fig. 1(b)) [32]. In the $SrFBiS_2$ type, carrier concentration at the BiS_2 layers can be tuned by the partial substitution of Sr by La [33,34]. These two kinds of blocking layers are quite similar to those of the Fe-based superconductors, LaFeAsO and SrFeAsF [8,35–37]. Basically, the blocking layers found in the Fe-based family could be formed in the BiS_2-based layered compounds as well. The common tendency of the crystal structure is a great advantage in exploring new BiS_2-based superconductors. The other crystal structure is $Bi_4O_4(SO_4)Bi_2S_4$ (Fig. 1(c)) [19]. In this crystal structure, it has been suggested that there are some defects at the SO_4 site, which cause the generation of electron carriers within the BiS_2 layers. Thus, the superconducting phase is $Bi_4O_4(SO_4)_{1-x}Bi_2S_4$.

3. Evolution of superconducting states in the BiS_2 layers

3.1. Superconductivity in $Bi_4O_4S_3$

The first member of the BiS_2-based superconducting family is $Bi_4O_4S_3$ with its crystal structure depicted in Fig. 1(c) [19]. The nominal composition of $Bi_4O_4S_3$ corresponds to the case of $x=0.5$ in $Bi_4O_4(SO_4)_{1-x}Bi_2S_4$. Namely, the superconducting phase of $Bi_4O_4S_3$ has a deficiency of 50% of the SO_4 ions. Band calculations suggest that the phase with no defects, $x=0$ ($Bi_6O_8S_5$), is an insulator with a band gap [19]. Then, the SO_4 deficiency generates electron carriers within the BiS_2 layers. With increasing concentration of the defects (x), $Bi_4O_4(SO_4)_{1-x}Bi_2S_4$ is expected to become metallic on the basis of the band calculations. In the metallic phase, superconductivity with a $T_c \sim 5$ K is observed. Fig. 2(a) shows the temperature dependence of magnetic susceptibility for the polycrystalline sample of $Bi_4O_4S_3$. The large diamagnetic signals indicate the evolution of bulk superconducting states below T_c. Fig. 2(b) shows the temperature dependence of electrical resistivity. The onset of T_c (T_c^{onset}) is ~ 5 K, and a zero-resistivity state is observed below 4.5 K. It should be noted that the resistivity begins to decrease gradually below 8.6 K, indicating that there is an inhomogeneity of the T_c. As shown in Fig. 2(c), the specific heat also shows evidence of bulk superconductivity below ~ 4.5 K in $Bi_4O_4S_3$ [38]. The estimated electron specific heat coefficient is very small, indicating that the electronic states of the $Bi_4O_4S_3$ superconductors are different from that of a normal metal. Furthermore, this tendency seems to be a common feature in the BiS_2 family, and the appearance of superconductivity in low-carrier states is similar to the case of electron-doped HfNCl or ZrNCl [39–41].

3.2. Superconductivity in $LaO_{1-x}F_xBiS_2$

At present, the studies of BiS_2-based superconductors have focused on the $REOBiS_2$ type because high-quality samples (single and poly crystals) can be prepared. Furthermore, the physical properties, such as superconductivity and magnetism, dramatically changes when changing the RE elements of the blocking layer. Here, the mechanisms for the appearance of superconductivity in the BiS_2 layers are introduced in detail, focusing on the $LaO_{1-x}F_xBiS_2$ system.

The parent compound $LaOBiS_2$ is not a superconductor. Band calculations and low-temperature transport measurements indicate that $LaOBiS_2$ is an insulator with a band gap [42–48]. Fig. 3(a)

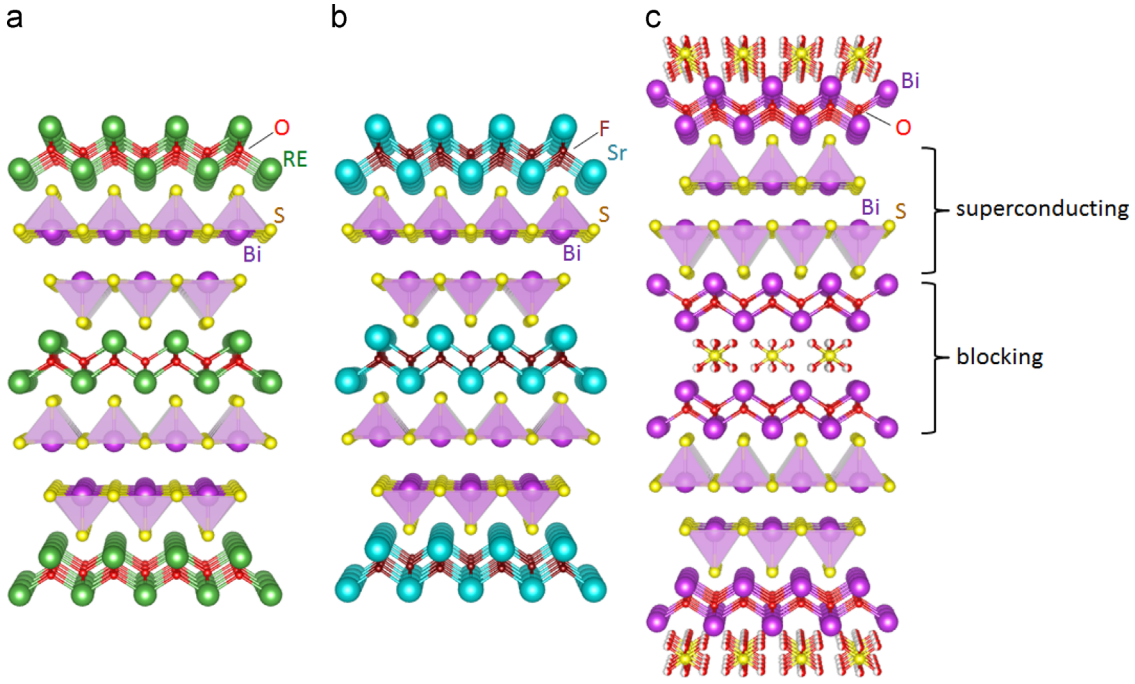

Fig. 1. Schematic images of the crystal structure of (a) $LaOBiS_2$, (b) $SrFBiS_2$ and (c) $Bi_4O_4(SO_4)Bi_2S_4$.

displays the first-principles band structure for $LaOBiS_2$ calculated without the spin-orbit coupling. As shown in Fig. 3(b), the $LaOBiS_2$ system is predicted to be metallic when electron carriers were doped within the BiS_2 layers. The Fermi energy for the doping ratio $\delta=0$, 0.25 and 0.5 is indicated in Fig. 3(b). Here δ is defined as the number of doped electrons per Bi site [42]. An effective method for doping electrons into the BiS_2 conduction layer is the partial substitution of the O site at the blocking layer by F. Due to the difference in the valency between O^{2-} and F^-, electron doping into the BiS_2 layers is expected; the same electron-doping method has been used in the FeAs-based superconductors [8]. Fig. 4 shows the X-ray diffraction (XRD) pattern and the calculated lattice constants for the F-substituted $LaOBiS_2$ ($LaO_{1-x}F_xBiS_2$) polycrystalline sample prepared using a conventional solid-state reaction. With increasing F concentration, the lattice volume decreases. The length of the *c* axis monotonously decreases with increasing *x*. In contrast, the *a* axis length does not show a remarkable change upon F substitution. For the $x=0.5$ ($LaO_{0.5}F_{0.5}BiS_2$) sample, the crystal structure analysis using Rietveld analysis indicates that the phase is of single phase with a tetragonal *P*4/*nmm* structure, as shown in Fig. 4(b) [20,49]. As expected above, the F-substituted $LaOBiS_2$ becomes metallic and shows a superconducting transition. The temperature dependence of electrical resistivity for $LaOBiS_2$ and $LaO_{0.5}F_{0.5}BiS_2$ is shown in Fig. 5. The non-doped $LaOBiS_2$ shows semiconducting behavior: the resistivity increases with decreasing temperature. The resistivity for $LaO_{0.5}F_{0.5}BiS_2$ is obviously smaller than that of $LaOBiS_2$, indicating that electron carriers are provided. $LaO_{0.5}F_{0.5}BiS_2$ exhibits a superconducting transition around 2.5 K. The best superconducting properties including the phase purity is obtained for *x*–0.5. With *x* higher than 0.5, impurity phases are detected in XRD. Fig. 6 shows the F concentration dependence of the calculated density of states [44]. The calculation results support the evolution of metallic nature upon F substitution. We note that the energy dependence of the density of states shows a peak around the Fermi energy (E_F) for $x=0.375$ and 0.5. Superconductivity is possibly induced by the enhancement of the density of states. Although the observed T_c of 2.5 K (T_c^{zero} in the resistivity measurements) in the $LaO_{0.5}F_{0.5}BiS_2$ polycrystalline sample was lower than what is expected, a slight diamagnetic signal was observed in the magnetization measurements below 10 K. To examine the possibility of a higher T_c, *high-pressure annealing* was performed. The polycrystalline samples prepared by a conventional solid-state reaction (for example, by heating at 800 °C for 15 h) were additionally annealed under a high pressure (HP) of 2 GPa at 600 °C for 1 h in a Cubic-anvil-type HP synthesis apparatus. The chart explaining the "HP annealing" is displayed in Fig. 7; here we distinguish the two kinds of samples as "As-grown" and "HP-annealed" samples.

Fig. 8 shows the temperature dependence of resistivity for the As-grown and HP-annealed $LaO_{0.5}F_{0.5}BiS_2$ polycrystalline samples. The T_c^{onset} dramatically increases from 3 K to 10.6 K by HP annealing. The T_c^{zero} is increased from 2.5 K to 7.8 K [20]. Furthermore, the superconducting volume fraction estimated using the shielding property in the magnetization measurements is also enhanced. These results indicate that there are some factors which interfere with the intrinsic nature of the superconductivity in $LaO_{0.5}F_{0.5}BiS_2$ for the As-grown sample. However, the intrinsic superconducting

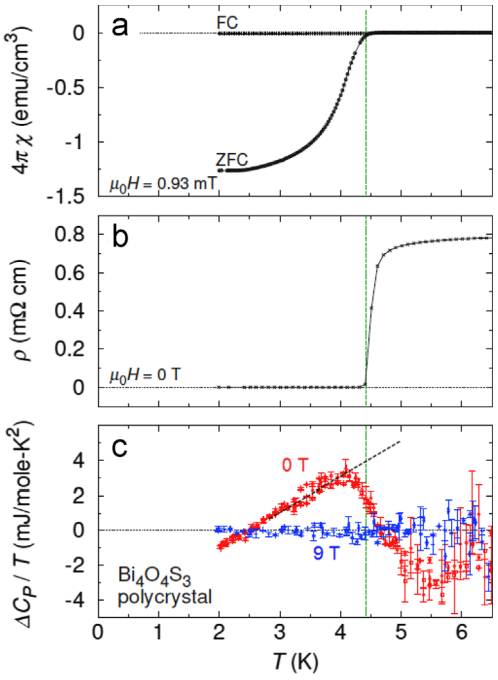

Fig. 2. Temperature dependence of (a) magnetic susceptibility, (b) electrical resistivity and (c) $\Delta C_p/T$ for the superconductor $Bi_4O_4S_3$ [19,38].

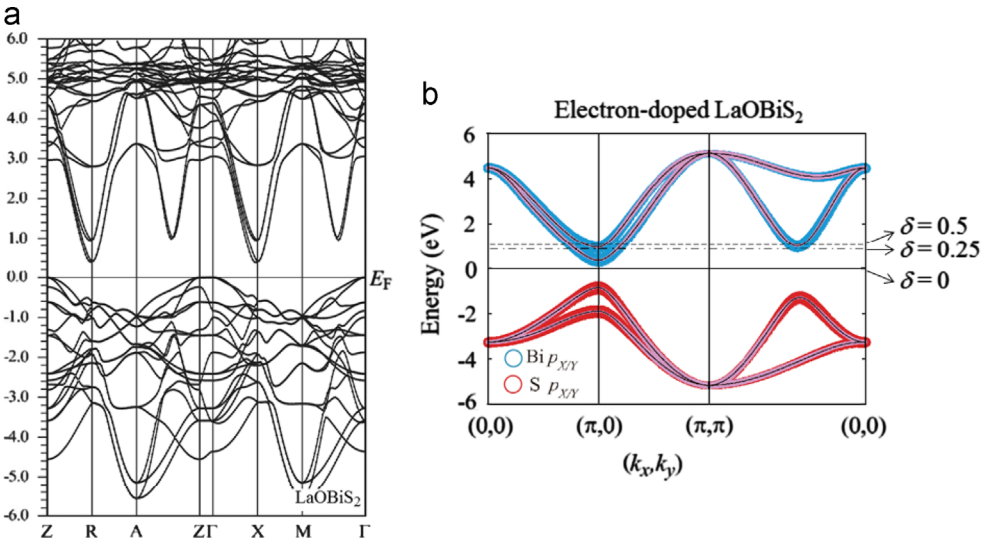

Fig. 3. (a) First-principles band structure of $LaOBiS_2$. (b)The four orbital model for $LaOBiS_2$. In (b), the dashed (dotted-dashed) lines denote the Fermi energy for the doping ratio $\delta=0.5$ ($\delta=0.25$). Here δ is defined as the number of doped electrons per Bi site, and satisfies $\delta=x$ in an ideal situation in $LaO_{1-x}F_xBiS_2$. [42] Reprinted from H. Usui, K. Suzuki, K. Kuroki, Phys. Rev. B 86 (2012) 220501. Copyright 2012 by American Physical Society.

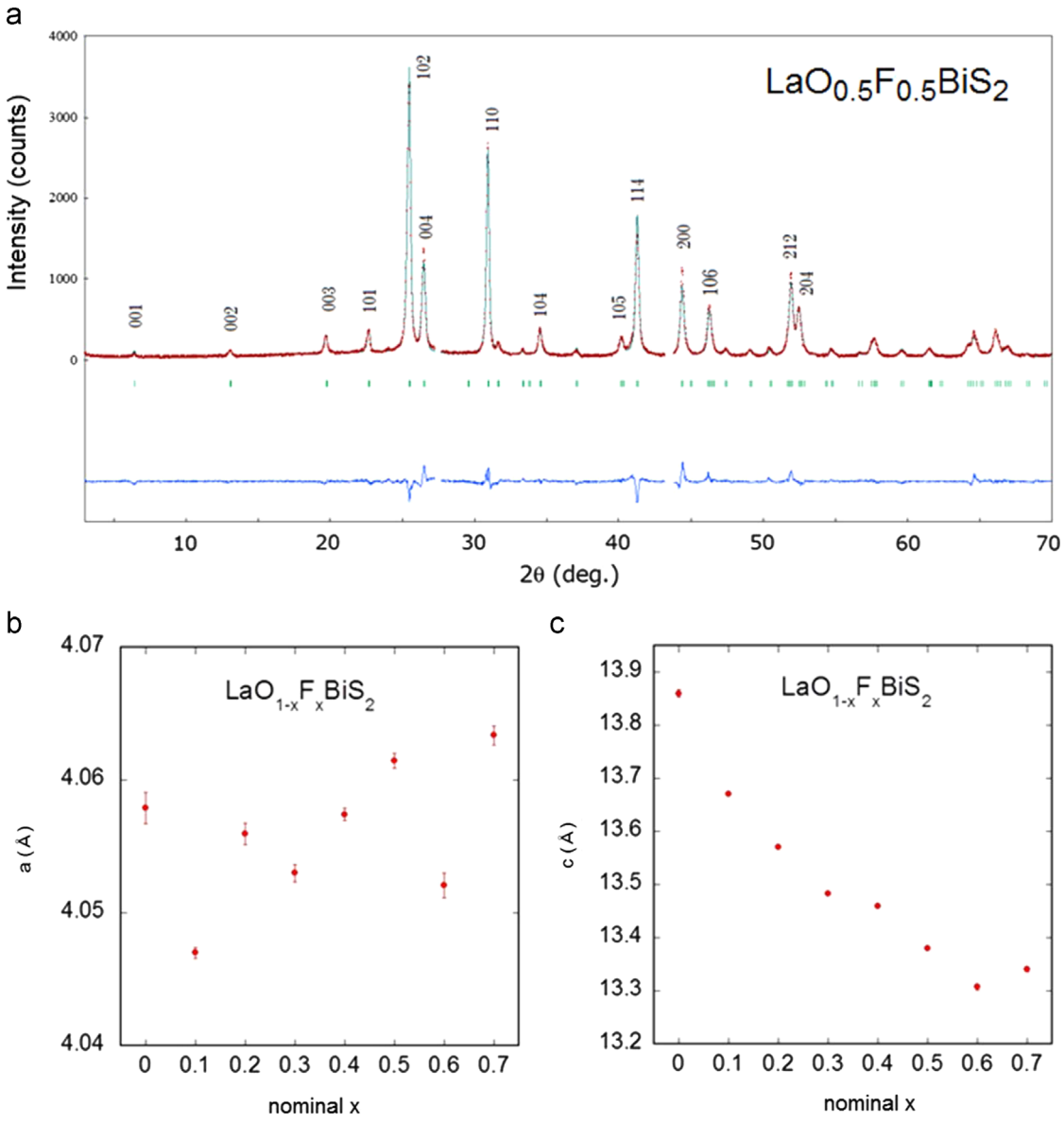

Fig. 4. (a) X-ray diffraction pattern and result of Rietveld refinements for $LaO_{0.5}F_{0.5}BiS_2$. (b) F concentration dependence on the lattice constant of the *a* axis. (c) F concentration dependence on the lattice constant of the *c* axis [20].

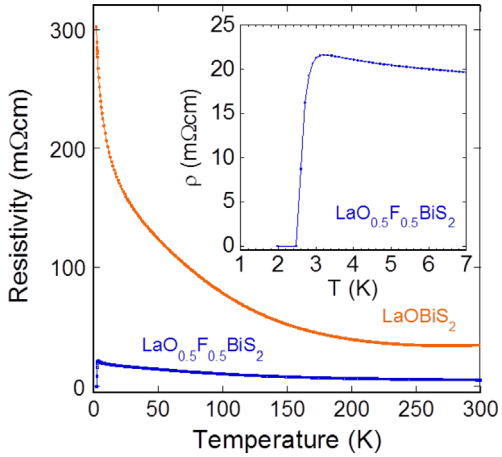

Fig. 5. Temperature dependences of electrical resistivity for $LaOBiS_2$ and $LaO_{0.5}F_{0.5}BiS_2$. The inset shows an enlargement of the temperature dependence of resistivity around the superconducting transition of $LaO_{0.5}F_{0.5}BiS_2$.

states can be induced when the HP annealing removes these factors. It was found that the superconducting properties for not only $x=0.5$ but also all the $LaO_{1-x}F_xBiS_2$ can be enhanced by applying HP annealing. Fig. 9 shows the temperature dependence of resistivity for the HP-annealed samples for $x=0$–0.7. Using these results, we obtain a superconductivity phase diagram, Fig. 10 [20,50,51]. The superconducting dome for the As-grown samples exhibits a lower T_c, and that for the HP-annealed samples clearly shows a higher T_c with a maximum at $x=0.5$.

Another method to dope electron carriers into the BiS_2 layers of $LaOBiS_2$ is a partial substitution of La by metals with a valence of 4+. Yazici et al. showed that $LaOBiS_2$ substituted with Th^{4+}, Hf^{4+}, Zr^{4+} or Ti^{4+} becomes superconducting [31]. Fig. 11 displays the temperature dependence of resistivity for $La_{1-x}M_xOBiS_2$ (M=Th, Hf, Zr and Ti). All four systems show a superconducting transition, and the observed T_c seems not to depend on the M elements. These findings suggest that superconductivity in the BiS_2 family is robust against elemental substitution as was found for the Fe-based superconductors.

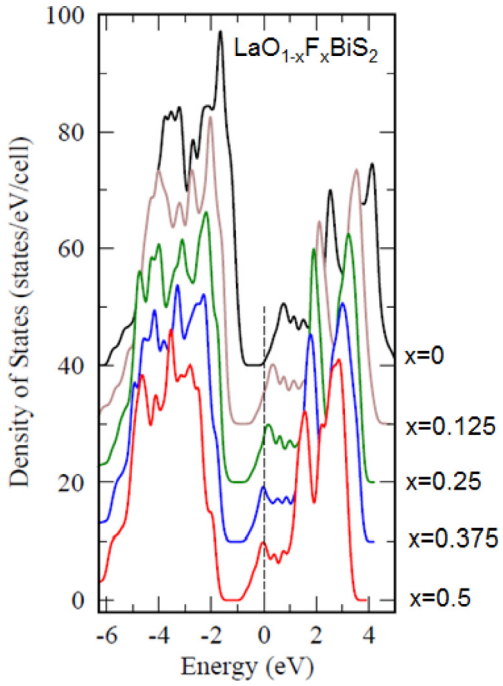

Fig. 6. Calculated density of states as a function of energy for $LaO_{1-x}F_xBiS_2$ [44]. Reprinted from T. Yildirim, Phys. Rev. B 87 (2013) 020506. Copyright 2013 by American Physical Society.

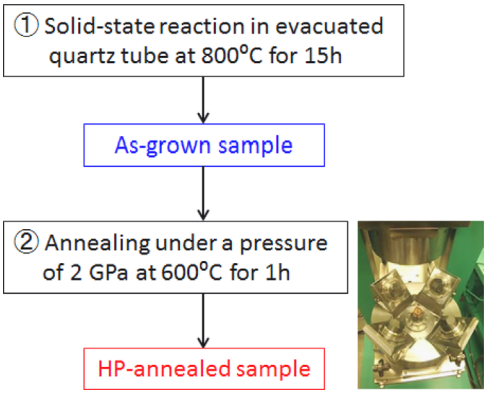

Fig. 7. Schematic chart of the HP-annealing process.

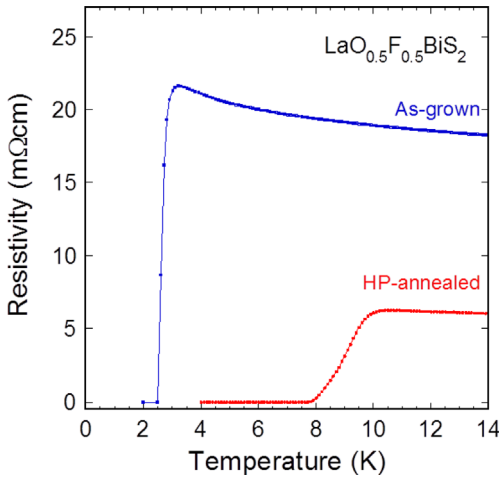

Fig. 8. Temperature dependences of electrical resistivity for As-grown and HP-annealed $LaO_{0.5}F_{0.5}BiS_2$ [20].

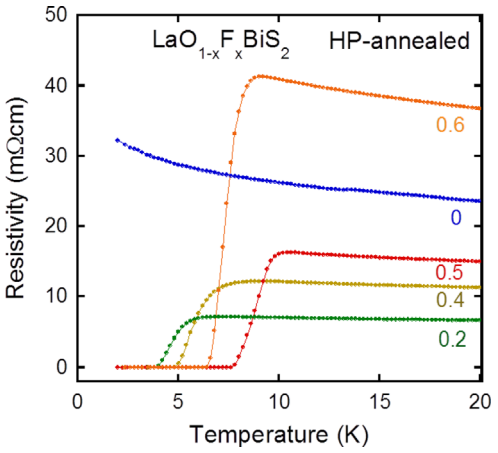

Fig. 9. Temperature dependences of electrical resistivity for HP-annealed $LaO_{1-x}F_x$-BiS_2 [50].

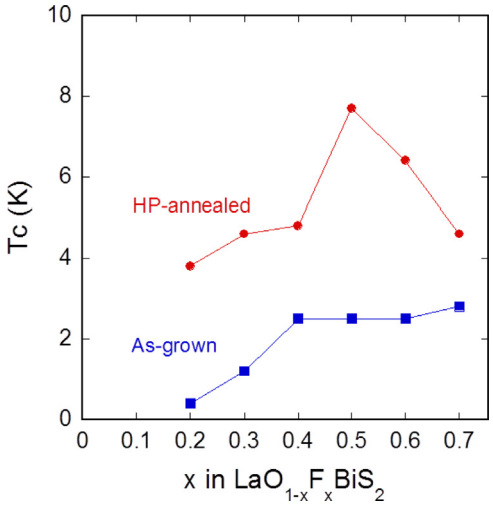

Fig. 10. Phase diagram of superconductivity for $LaO_{1-x}F_xBiS_2$ [20,50,51]. In this phase diagram, the T_c^{zero} in the resistivity measurements and the T_c^{irr} in the magnetization measurements are plotted.

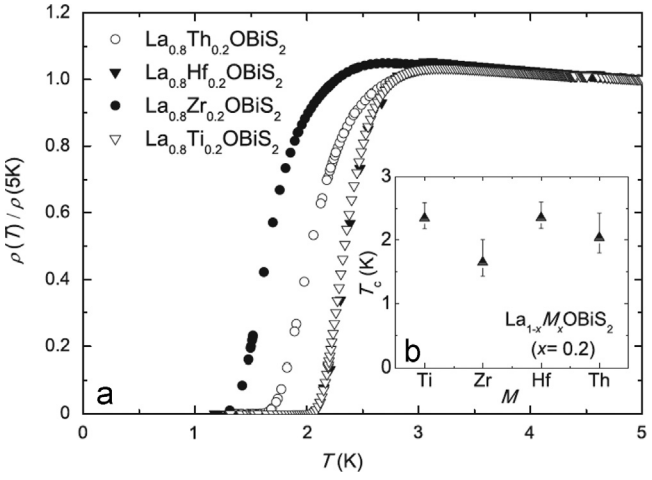

Fig. 11. Temperature dependences of electrical resistivity for $La_{0.8}Th_{0.2}OBiS_2$, $La_{0.8}Hf_{0.2}OBiS_2$, $La_{0.8}Zr_{0.2}OBiS_2$ and $La_{0.8}Ti_{0.2}OBiS_2$ [31]. Reprinted from D. Yazici, K. Huang, B.D. White, I. Jeon, V.W. Burnett, A.J. Friedman, I.K. Lum, M. Nallaiyan, S. Spagna, M.B. Maple, Phys. Rev. B 87 (2013) 174512. Copyright 2013 by American Physical Society.

The evolution of superconductivity in the $LaOBiS_2$ system is summarized. The parent phase is an insulator, and hence, the doping of electron carriers into the BiS_2 layers is required for the inducement of superconductivity. The partial substitution of O with F is one of the effective ways to dope electrons into the BiS_2 layers, and the F-substituted $LaOBiS_2$ shows a superconducting transition at low temperatures. Another way to dope electrons is by partial substitution of La by Th, Hf, Zr or Ti. In the case of $LaO_{1-x}F_xBiS_2$, the superconducting properties are dramatically improved by the HP-annealing process, and the best superconducting properties, $T_c^{onset}=10.6$ K and $T_c^{zero}=7.8$ K, are obtained for the HP-annealed sample of $LaO_{0.5}F_{0.5}BiS_2$. A detailed investigation of the relationship between the increase in T_c and changes in the crystal structure will be shown later in Section 4.

3.3. *Superconductivity in $REO_{1-x}F_xBiS_2$*

In the $REOBiS_2$-type structure, we have so far five choices when synthesizing BiS_2-based superconductors. As introduced above, $LaOBiS_2$ becomes superconducting via electron doping. The La site can be replaced by Ce, Pr, Nd or Yb. Here, the physical properties of various $REO_{1-x}F_xBiS_2$ are briefly introduced.

The $CeOBiS_2$ system is one of the most notable systems because the superconducting states at the BiS_2 layers and the magnetic ordering of Ce at the blocking layers coexist. Xing et al. firstly synthesized the $CeO_{1-x}F_xBiS_2$ polycrystalline samples [24]. The electrical resistivity measurements revealed that superconducting transitions are observed for $x \geq 0.3$ in $CeO_{1-x}F_xBiS_2$, and T_c reaches 3 K. However, large diamagnetic signals were not observed in the magnetization measurements, indicating that the observed superconducting states were not bulk in nature in the As-grown samples of $CeO_{1-x}F_xBiS_2$ (see Fig. 12(a,b)). The notable feature in $CeO_{1-x}F_xBiS_2$ is the observation of the magnetic ordering which was suggested to be a result of the ferromagnetic ordering of the Ce moment. If the magnetic ordering at the CeO layer and the bulk superconducting states at the BiS_2 layers could occur simultaneously, the situation is curious on several aspects. Demura et al. showed that HP annealing can induce bulk superconductivity in $CeO_{1-x}F_xBiS_2$ as in the case of $LaO_{1-x}F_xBiS_2$ [25]. As shown in Fig. 12, the T_c of the HP-annealed samples of $CeO_{1-x}F_xBiS_2$ obviously increases. The maximum T_c is 3 K for the As-grown samples and 6 K for the HP-annealed samples in the resistivity measurements. Furthermore, the shielding volume fraction is also strongly enhanced in the HP-annealed samples, indicating the evolution of bulk superconducting states. Interestingly, the signals of the magnetic ordering of Ce still exist. Hence, the magnetic ordering at the CeO layer and the bulk superconducting states at the BiS_2 layers occur simultaneously in the HP sample. Although the magnetic structure of $CeO_{1-x}F_xBiS_2$ has not been clarified yet, it is clear that magnetism and superconductivity coexist in the HP-annealed $CeO_{1-x}F_xBiS_2$ samples. In addition, we note an interesting tendency of T_c and the magnetic transition temperature with F concentration. Fig. 13(a) is a magnetic phase diagram for HP-annealed $CeO_{1-x}F_xBiS_2$ showing the magnetic transition temperature as a function of x. There are two kinds of ferromagnetic transition temperatures of 4.5 K and 7.5 K. The 7.5 K phase appears at a higher F concentration of $x > 0.6$. Fig. 13(b) is a superconducting phase diagram for HP-annealed $CeO_{1-x}F_xBiS_2$ showing the T_c^{zero} as a function of x. Bulk superconductivity with a higher T_c appears at a higher F concentration of $x > 0.6$. Interestingly, these two phase diagrams show a similar shape. Although it might have corresponded incidentally, it is quite interesting to consider that

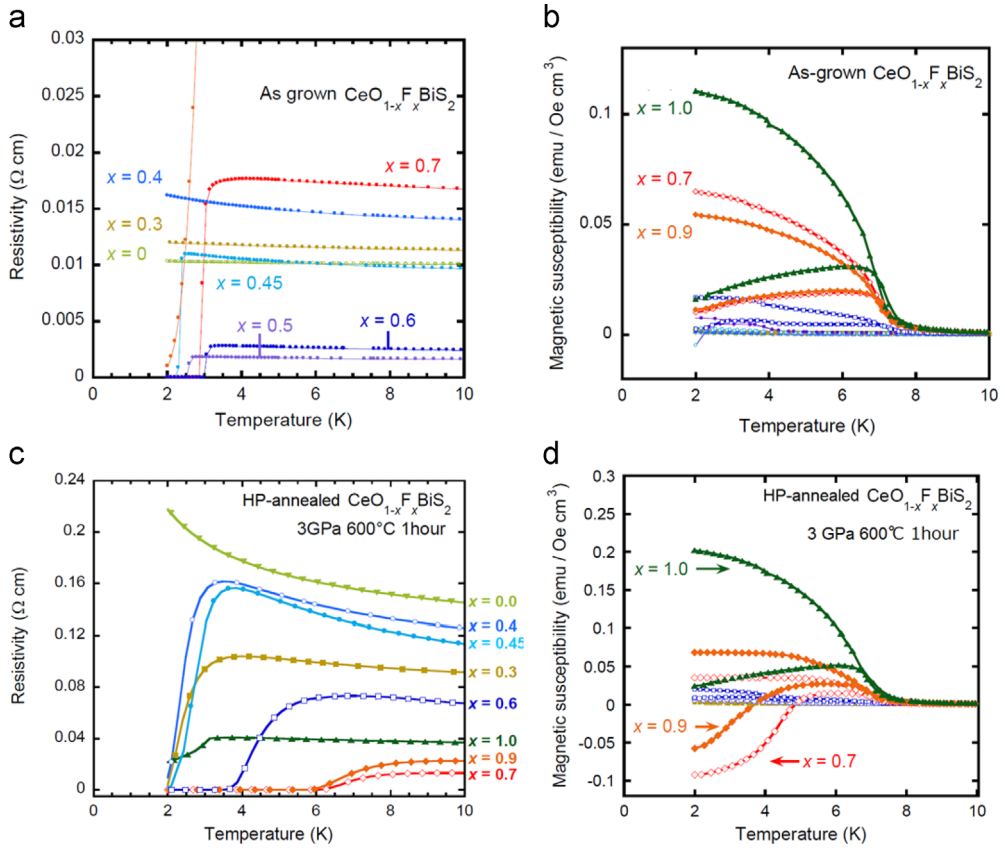

Fig. 12. (a) Temperature dependences of electrical resistivity for As-grown $CeO_{1-x}F_xBiS_2$. (b) Temperature dependences of magnetic susceptibility for As-grown $CeO_{1-x}F_xBiS_2$. (c) Temperature dependences of electrical resistivity for HP-annealed $CeO_{1-x}F_xBiS_2$. (d) Temperature dependences of magnetic susceptibility for HP-annealed $CeO_{1-x}F_xBiS_2$. [25].

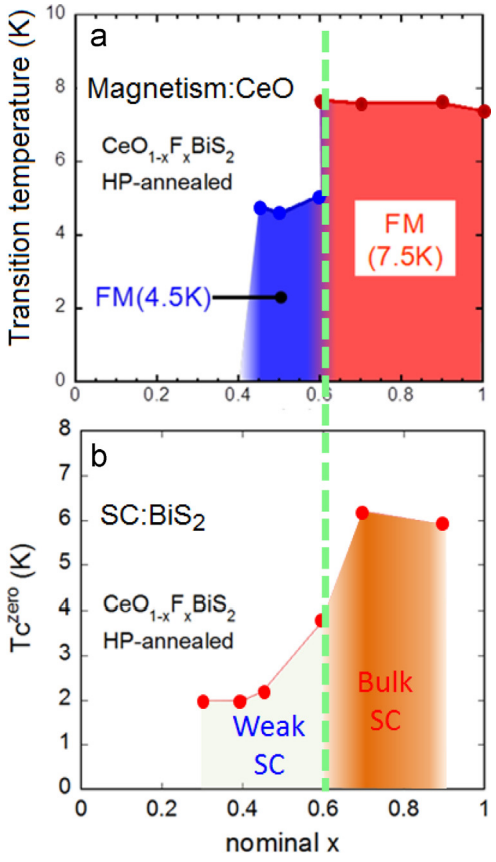

Fig. 13. (a) Phase diagram of magnetic ordering for the CeO blocking layers for HP-annealed $CeO_{1-x}F_xBiS_2$. (b) Phase diagram of superconductivity within the BiS_2 layers for HP-annealed $CeO_{1-x}F_xBiS_2$. [25].

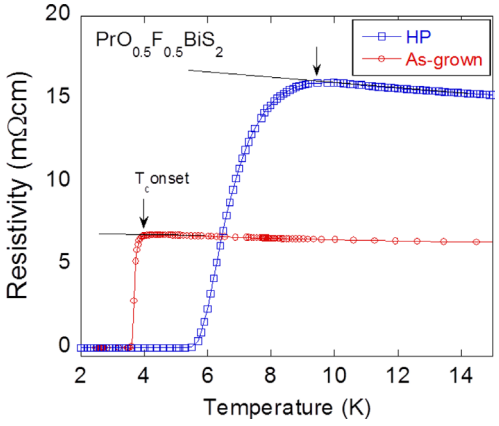

Fig. 14. Temperature dependences of electrical resistivity for As-grown and HP-annealed $PrO_{0.5}F_{0.5}BiS_2$ [27].

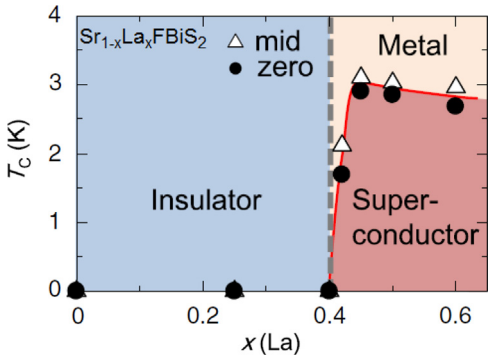

Fig. 15. Phase diagram of superconductivity for $Sr_{1-x}La_xFBiS_2$ [34]. Reprinted from H. Sakai, D. Kotajima, K. Saito, H. Wadati, Y. Wakisaka, M. Mizumaki, K. Nitta, Y. Tokura, S. Ishiwata, J. Phys. Soc. Jpn. 83 (2014) 014709. Copyright 2014 by The Physical Society of Japan.

superconductivity of the BiS_2 layers and magnetic ordering of the blocking layers are linked via some factors, for example, local crystal structures. To clarify the correlation, further investigations using neutron scattering, μSR or the other experiments sensitive to the evolution of magnetic ordering are required.

Superconductivity in the $PrOBiS_2$ system was reported by Jha et al. and Yazici et al. [26,30]. As in the former cases of the La and Ce systems, superconductivity is induced by a partial substitution of O by F. The polycrystalline samples of $PrO_{0.5}F_{0.5}BiS_2$ show bulk superconductivity below 3 or 4 K with a large shielding volume fraction in the magnetization measurements. Namely, the As-grown samples show bulk superconductivity. However, the T_c of $PrO_{0.5}F_{0.5}BiS_2$ can be increased by applying HP annealing as well [27]. Fig. 14 displays the temperature dependence of resistivity for the As-grown and HP-annealed samples of $PrO_{0.5}F_{0.5}BiS_2$. The T_c^{onset} is increased from 4.0 K to 9.4 K, and the T_c^{zero} increased from 3.6 K to 5.5 K by applying HP annealing.

The $NdO_{1-x}F_xBiS_2$ system is the most suitable material for discussing the properties at ambient pressure [28]. The reason is that the single-phase samples which show bulk superconductivity with a T_c of ~5.5 K, which is the highest (optimized value) in this system, by a solid-state reaction at ambient pressure, namely, without any high-pressure synthesis technique. The difference in the condition of the appearance of superconductivity in between the $LaOBiS_2$ and the $NdOBiS_2$ systems would be understood by the chemical pressure effects which is tuned by changing the RE elements at the blocking layers. With decreasing ionic radius from La^{3+} to Nd^{3+}, the lattice volume is largely compressed. Hence, bulk superconductivity in $NdO_{1-x}F_xBiS_2$ can be realized without any HP annealing.

The last superconductor with the $REOBiS_2$-type structure is $YbO_{0.5}F_{0.5}BiS_2$ [30]. Yazici et al. succeeded in the observation of a superconducting transition with a relatively high T_c of 5.3 K. Furthermore, antiferromagnetic signals are observed in the magnetization measurements. This system should be of interest if there is the coexistence of magnetism and superconductivity as was observed in the case of $CeO_{1-x}F_xBiS_2$. However, the superconducting signals in the magnetization measurements are quite small. The lack of bulk superconductivity may be due to the excess effect of chemical pressure caused by the small ionic radius of Yb^{3+}. If the crystal structure could be optimized for the appearance of bulk superconductivity, $YbO_{1-x}F_xBiS_2$ will be a more interesting system.

3.4. Superconductivity in $Sr_{1-x}La_xFBiS_2$

As shown in Fig. 1(b), the REO layers in Fig. 1(a) can be replaced by the SrF layers as well as in the Fe-based superconductors [35–37]. Lei et al. reported that the parent phase $SrFBiS_2$ is an insulator on the basis of the resistivity measurements and band calculations [32]. Soon after the report, Lin et al. showed that a partial substitution of Sr^{2+} by La^{3+} induces metallic conductivity and a superconducting transition below 3 K in $Sr_{0.5}La_{0.5}FBiS_2$ [33]. Fig. 15 is a phase diagram of $Sr_{1-x}La_xFBiS_2$ established by Sakai et al. [34]. According to the phase diagram, a metal–insulator transition occurs at around $x=0.4$, and a superconducting phase is induced. Interestingly, the highest T_c is observed at $x=0.45$, which is close to the metal–insulator boundary. On the basis of thermodynamic measurements, it was suggested that the superconducting coupling strength is enhanced

when approaching the metal–insulator boundary. These features of superconductivity in $Sr_{1-x}La_xFBiS_2$ resemble those for the electron-doped ZrNCl (or HfNCl) superconductors, which have been known as low-carrier superconductors [39–41]. The possibility of low-carrier superconductivity in the BiS_2 family was suggested in the specific heat studies for $Bi_4O_4S_3$ [38]. If the feature of low-carrier superconductivity is intrinsic in the BiS_2 family, we will be able to discuss the mechanisms of the appearance of superconductivity in the low-carrier metallic states by investigating various types of BiS_2-based superconductors.

4. Pressure effect

4.1. High pressure annealing effect

As introduced in Section 3, the superconducting properties of $REOBiS_2$-type superconductors can be enhanced by HP annealing [20,50]. In fact, the crystal structure under high pressure can be kept after the HP annealing in the $REOBiS_2$-type materials. The HP-annealed samples have given us some fruitful information for discussing the relationship between superconducting properties and crystal structure.

In $LaO_{1-x}F_xBiS_2$, the T_c^{onset} increases from ~3 K to ~11 K by HP annealing. The increase of T_c is accompanied with structural changes [52]. Fig. 16 shows the enlargements of the XRD patterns near around the (004) and (200) peaks for the As-grown and HP samples of $LaO_{0.5}F_{0.5}BiS_2$. It is clear that the lattice structure has changed by HP annealing. The (004) peak obviously shifts to a higher angle while the (200) peak slightly shifts to a lower angle. These peak shifts indicate that the *a* axis is slightly expanded while the *c* axis is largely contracted by HP annealing. In $LaO_{0.5}F_{0.5}BiS_2$, the increase of T_c could be explained by the uniaxial lattice shrinkage along the *c* axis, which could optimize the local crystal structure.

Similar tendency is observed in the $PrO_{0.5}F_{0.5}BiS_2$ superconductors [27]. As shown in Fig. 14, the T_c^{zero} of As-grown $PrO_{0.5}F_{0.5}BiS_2$ is 3.6 K. The T_c could be increased up to $T_c^{zero}=5.5$ K and $T_c^{onset}=9.4$ K by HP annealing. The enhancement of T_c is related to the uniaxial lattice contraction as well as in $LaO_{0.5}F_{0.5}BiS_2$. Fig. 17 shows the enlargements of the XRD patterns near around the (004) and (200) peaks for the As-grown and HP samples of $PrO_{0.5}F_{0.5}BiS_2$. The (004) peak clearly shifts to a higher angle which indicates that the *c* axis is contracted by HP annealing. In contrast, the (200) peak does not show a remarkable change in the peak position. Namely, only the *c* axis length decreased by HP annealing. On the basis of these changes in lattice constants and superconducting properties, the uniaxial lattice contraction seems to be essential to induce a higher T_c in the $REO_{1-x}FxBiS_2$ system.

4.2. High pressure studies

Another effective way to enhance the superconducting properties of BiS_2-based superconductors is application of external high pressure. By using a HP cell, we can tune the applied pressure,

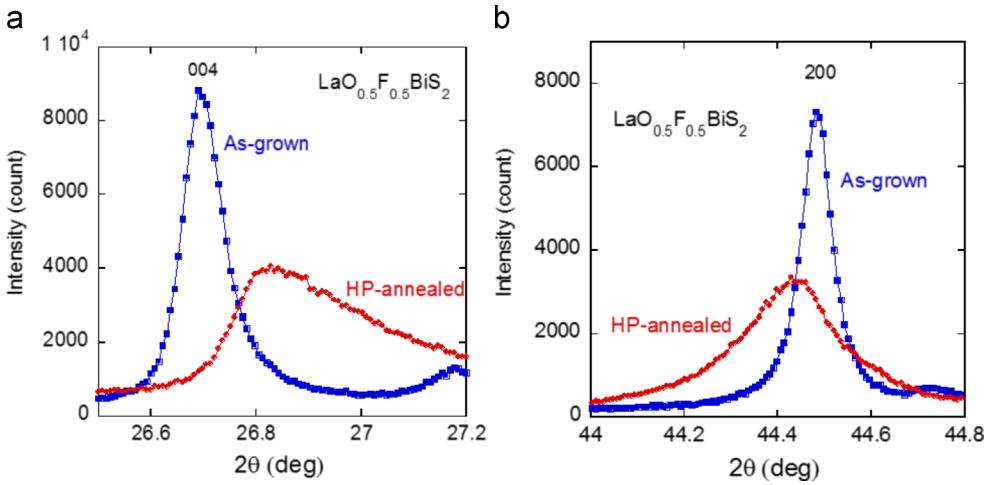

Fig. 16. (a) Enlargement of X-ray diffraction patterns of As-grown and HP-annealed $LaO_{0.5}F_{0.5}BiS_2$ around the (004) peak. (a) Enlargement of x-ray diffraction patterns of As-grown and HP-annealed $LaO_{0.5}F_{0.5}BiS_2$ around the (200) peak. [52].

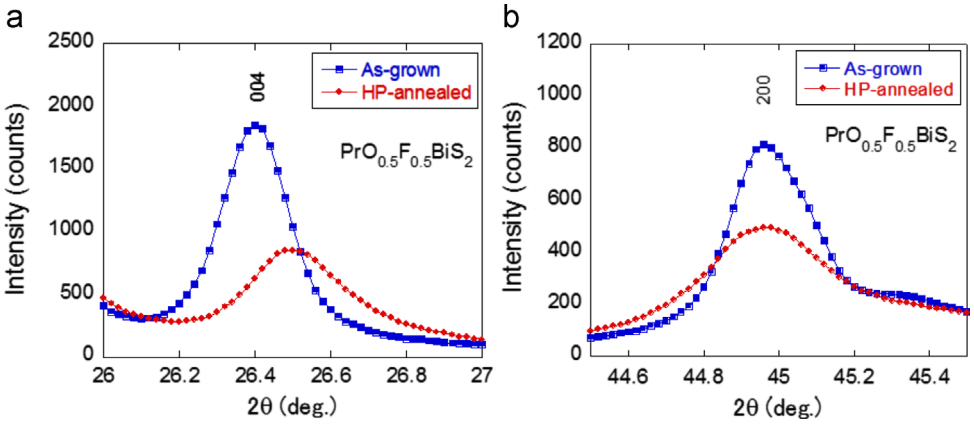

Fig. 17. (a) Enlargement of X-ray diffraction patterns of As-grown and HP-annealed $PrO_{0.5}F_{0.5}BiS_2$ around the (004) peak. (a) Enlargement of X-ray diffraction patterns of As-grown and HP-annealed $PrO_{0.5}F_{0.5}BiS_2$ around the (200) peak. [27].

which allows us to discuss the continuous changes in crystal structure and physical properties. The most outstanding enhancement of superconducting properties is observed in $LaO_{0.5}F_{0.5}BiS_2$ [53]. As mentioned above, the T_c of As-grown $LaO_{0.5}F_{0.5}BiS_2$ is less than 3 K. As shown in Fig. 18, the T_c largely raises up to over 10 K by applying a high pressure of 0.6 GPa. Then, the T_c gradually decreases with increasing pressure. The rapid increase in T_c around 0.6 GPa suggests that there is a phase transition from a lower-T_c phase to higher-T_c phase of $LaO_{0.5}F_{0.5}BiS_2$. Tomita et al. carried out crystal structure analysis for As-grown $LaO_{0.5}F_{0.5}BiS_2$ using XRD under high pressure and density functional calculations. They concluded that there is a pressure-induced structure phase transition from tetragonal to monoclinic as depicted in Fig. 19. In the proposed monoclinic phase, the double BiS_2 layers move and the Bi–Bi distance in each layer becomes shorter. The enhancement of T_c in $LaO_{0.5}F_{0.5}BiS_2$ might be due to the change in electronic structure induced by the structural changes.

The T_c of the HP-annealed $LaO_{0.5}F_{0.5}BiS_2$ sample, T_c^{zero}–8 K, also increases up to over 10 K by applying external pressures [54]. The obtained maximum T_c is almost the same as that obtained for the As-grown sample under high pressures. The pressure dependences of T_c for the As-grown and HP-annealed $LaO_{0.5}F_{0.5}BiS_2$ samples are plotted together in Fig. 20. It is interesting that the two curves overlap with each other above 1 GPa. Therefore, it can be considered that the effect of HP annealing or external pressure is almost the same with respect to the superconducting properties.

Fig. 20 includes the pressure dependences of T_c for the other $REOBiS_2$-type superconductors as well [53–56]. Almost all the BiS_2-based superconductors show a transition-like behavior for the pressure dependence of T_c: the T_c abruptly increases at a characteristic pressure. In the $REOBiS_2$-type materials, the characteristic pressure increases when decreasing the ionic radius of rare earth, namely in the order of La, Ce, Pr and Nd. The $Sr_{1-x}La_xFBiS_2$ also shows such behavior in the pressure dependence of T_c [57]. The T_c of $Sr_{1-x}La_xFBiS_2$ at ambient pressure is 2 K. It abruptly increases to 10 K above ~1 GPa, which is almost the same pressure range where $LaO_{0.5}F_{0.5}BiS_2$ shows an increase of T_c. Having compared the pressure dependences of T_c and the crystal structure, we note that the pressure where the T_c increases seems

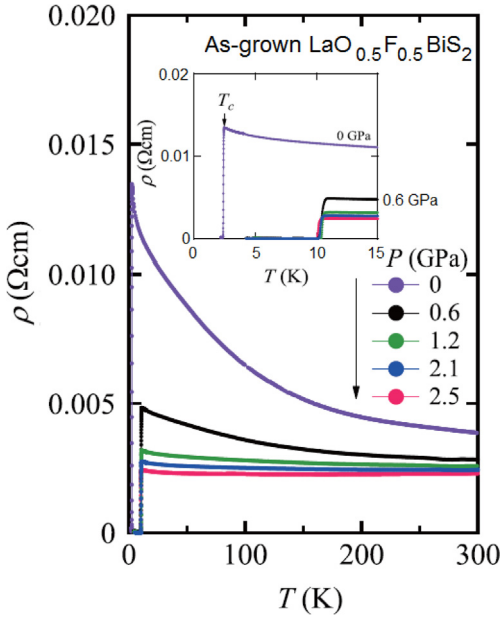

Fig. 18. Temperature dependences of electrical resistivity for $LaO_{0.5}F_{0.5}BiS_2$ under pressures of 0, 0.6, 1.2, 2.1 and 2.5 GPa [53]. The inset shows an enlarged figure of below 15 K.

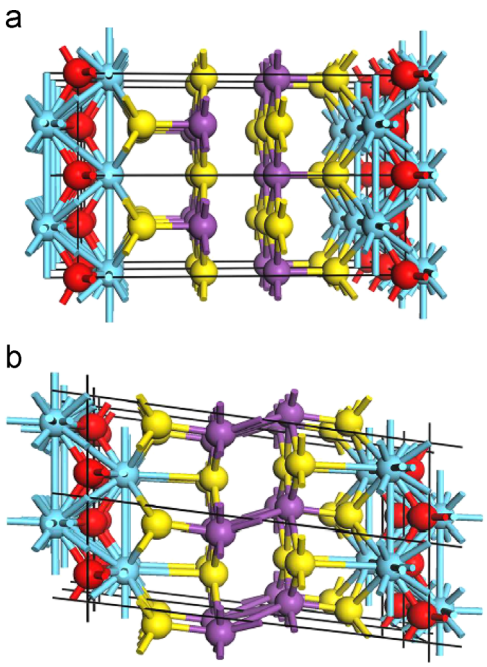

Fig. 19. Schematic images of the crystal structure of $LaO_{0.5}F_{0.5}BiS_2$ under (a) ambient pressure (tetragonal) and (b) high pressure (monoclinic) [53].

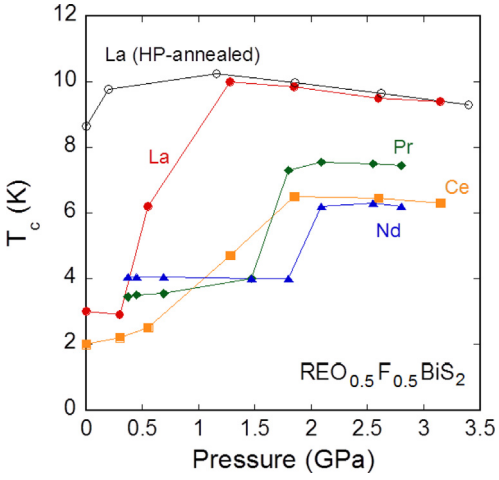

Fig. 20. Pressure dependences of T_c for $REO_{0.5}F_{0.5}BiS_2$ (RE=La, Ce, Pr and Nd).

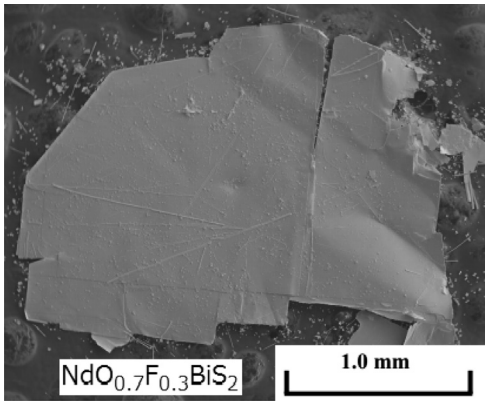

Fig. 21. Photograph of $NdO_{0.7}F_{0.3}BiS_2$ single crystals [58].

to depend on the *a* axis length. These facts provide us with a scenario where the characteristic pressure, probably a critical pressure of structural change, is depending on the size of the blocking layer in the $REOBiS_2$ and $SrFBiS_2$ systems. Contrary to the others, $Bi_4O_4S_3$ does not exhibit an increase in T_c under high pressure [54]. The difference in pressure effect may be related to its large blocking layer along the *c* axis (see Fig. 1(c)), which would affect the occurrence of structural change under high pressure. The thicker blocking layer may stabilize the tetragonal structure under high pressure.

5. Single crystal growth and large anisotropy of superconductivity

Recently, two groups reported successful single crystal growth of $REO_{1-x}F_xBiS_2$ superconductors [58–60]. Nagao et al. succeeded in growing $REO_{1-x}F_xBiS_2$ (RE=La, Ce and Nd) single crystals [58,59,61]. An image of a typical crystal of $NdO_{0.7}F_{0.3}BiS_2$ is shown in Fig. 21. Crystal structure analysis on these crystals proved that the tetragonal structure suggested in the structural analysis using polycrystalline samples were correct. One of the outstanding findings is a remarkably high anisotropy parameters (γ) of superconductivity, which is given by $\gamma=H_{c2}^{ab}/H_{c2}^{c}$, where H_{c2} is an upper critical field. Fig. 22(a) and (b) shows the temperature dependences of resistivity for the $NdO_{0.7}F_{0.3}BiS_2$ single crystal with applied magnetic fields parallel to

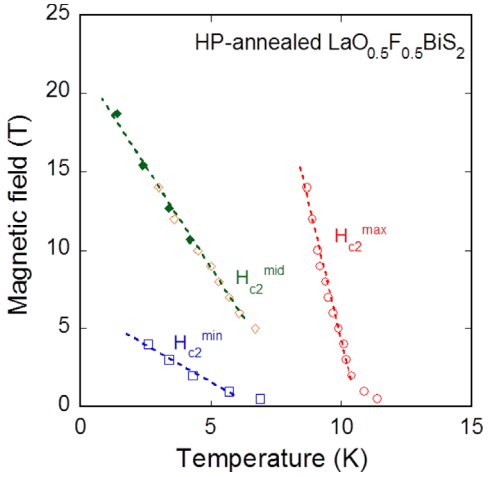

Fig. 23. Magnetic field–temperature phase diagram of HP-annealed $LaO_{0.5}F_{0.5}BiS_2$ [63].

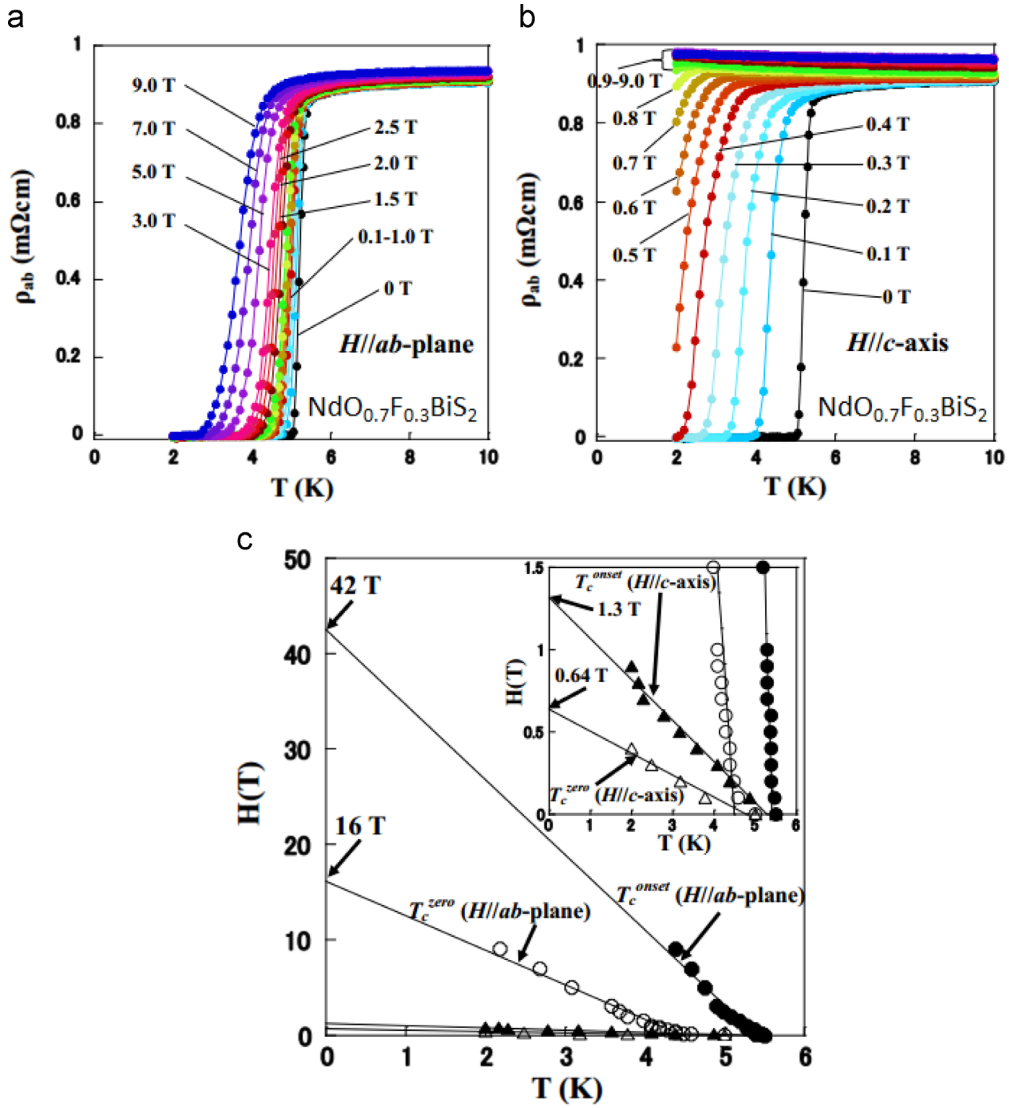

Fig. 22. (a) Temperature dependences of electrical resistivity for $NdO_{0.7}F_{0.3}BiS_2$ a single crystal under magnetic fields (*H*//*ab*) up to 9 T. (b) Temperature dependences of electrical resistivity for a $NdO_{0.7}F_{0.3}BiS_2$ single crystal under magnetic fields (*H*//*c*) up to 9 T. (c) Magnetic field–temperature phase diagram of $NdO_{0.7}F_{0.3}BiS_2$ [58].

the *ab* plane and the *c* axis, respectively. The magnetic field–temperature phase (*H*–*T*) diagram for the $NdO_{0.7}F_{0.3}BiS_2$ single crystal is shown in Fig. 22(c). The superconducting states are easily destroyed when *H*//*c* while superconductivity is robust when *H*//*ab*, indicating a large anisotropy of the superconductivity [58,60]. For $LaO_{1-x}F_xBiS_2$ and $NdO_{1-x}F_xBiS_2$ single crystals, the anisotropy parameter is 30–40 [60]. The estimated large anisotropy is comparable to that observed in Bi-based cuprates (high-T_c superconductors). The fact suggests that we will be able to fabricate some BiS_2-based superconducting devices by using the large anisotropy of superconductivity. One possibility is fabrication of intrinsic Josephson junctions which have been achieved using cuprates.

Differently from the cases of RE=La and Nd, the anisotropy parameter of $CeO_{1-x}F_xBiS_2$ has relatively smaller values of 13–21 [59]. Then, one question arises: is a large anisotropy advantageous for a higher T_c in the BiS_2 family? To discuss this relationship, comparison of anisotropy of superconductivity between higher-T_c and lower-T_c phases is needed. The $LaO_{0.5}F_{0.5}BiS_2$ superconductor is suitable to address this issue because the T_c for the As-grown (T_c^{onset} – 3 K) and HP-annealed (T_c^{onset} – 11 K) samples is very different. The anisotropy of the HP-annealed $LaO_{0.5}F_{0.5}BiS_2$ sample was investigated using the general method for estimation of anisotropy of superconductivity in the polycrystalline samples of layered superconductors [62]. Fig. 23 shows the *H*–*T* phase diagram of HP-annealed $LaO_{0.5}F_{0.5}BiS_2$ [63]. Three kinds of H_{c2} were observed. The lowest H_{c2} (H_{c2}^{min}) could be regarded as H_{c2}^{c}. The other two kinds of H_{c2} could be regarded as H_{c2}^{ab}. If there is monoclinic distortion or strain in the HP-annealed $LaO_{0.5}F_{0.5}BiS_2$ sample as discussed in Section 4, there should be anisotropy of superconducting states between the *a* axis and *b* axis. Furthermore, a theoretical study suggested that the BiS_2-based materials have one-dimensional characteristics in the electronic states. Thus, the two kinds of H_{c2} (H_{c2}^{max} and H_{c2}^{mid}) observed in the HP-annealed $LaO_{0.5}F_{0.5}BiS_2$ sample could be regarded as H_{c2}^{a} or H_{c2}^{b}. The anisotropy parameter estimated using the slopes of temperature dependence of H_{c2} for H_{c2}^{max} and H_{c2}^{min} is 7.4. The estimated value is clearly lower than that for the As-grown $LaO_{0.5}F_{0.5}BiS_2$ single crystal, $\gamma > 30$. Therefore, a larger anisotropy of superconductivity is not essential for the emergence of a higher T_c.

6. Electronic structure and possible paring symmetry

Superconductivity in the BiS_2-based materials emerges within the double BiS_2 layers. As introduced in Section 3, the parent phase is basically an insulator with a band gap. Doping electron carriers into the BiS_2 layers makes the materials metallic and induces superconducting states. In the case of the $REOBiS_2$ system, electron carriers could be generated by a partial substitution of O by F. Here, investigations of electronic states by means of photoemission spectroscopy (PES) including angle-resolved PES (ARPES) and scanning tunneling microscopy/scanning tunneling spectroscopy (STM/STS) are briefly introduced.

Nagira et al. carried out PES for the polycrystalline samples of $LaO_{1-x}F_xBiS_2$ [64]. Fig. 24 displays the valence band soft X-ray photoemission spectroscopy (SXPES) spectra for $LaO_{1-x}F_xBiS_2$. The electronic density of states near E_F is slightly enhanced upon F substitution, but the obtained density of states near E_F is obviously smaller than that expected by theoretical calculations. The low density of states seems to be consistent with the transport properties for the polycrystalline $LaO_{1-x}F_xBiS_2$ in which semiconducting-like temperature dependence of resistivity was observed. Furthermore, they suggested that the valence state of Bi became mixed-valence. There might be charge (valence) fluctuations in the BiS_2-based materials. If such fluctuations play an important role for the appearance of superconductivity, unconventional mechanisms of superconductivity should be considered.

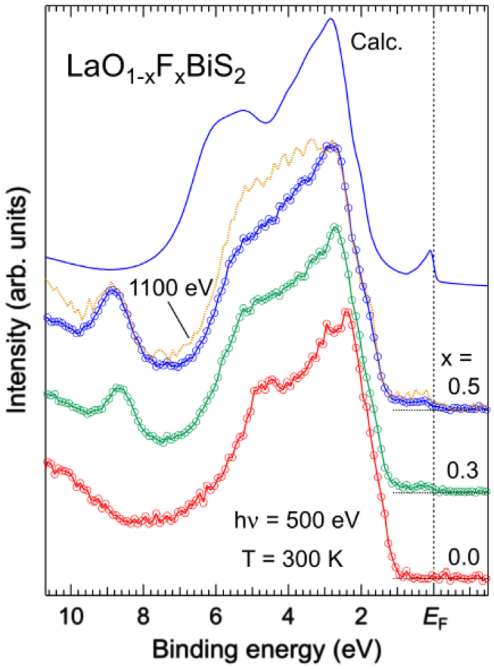

Fig. 24. Valence band soft X-ray photoemission spectroscopy (SXPES) spectra of $LaO_{1-x}F_xBiS_2$ (x=0.0, 0.3, and 0.5) obtained using 500 eV (open circles connected with lines) and 1100 eV (a broken line) photon energies (only for $LaO_{0.5}F_{0.5}BiS_2$) with a calculated spectrum [64].

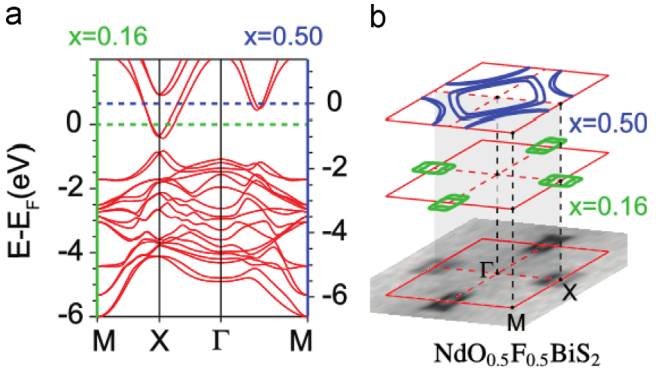

Fig. 25. (a) Calculated band structures without the spin-orbital coupling for $NdO_{1-x}F_xBiS_2$ with x=0.16 (the left side energy axis) and x=0.5 (the right side one). (b) Comparison of the Fermi-surface between the photoemission intensity map and the density-functional theory for x=0.5 and 0.16 fluorine substitution levels [65].

To obtain further information, ARPES is quite powerful. Recently, Ye et al. reported ARPES on $NdO_{0.5}F_{0.5}BiS_2$ single crystals (Fig. 25) [65]. The obtained ARPES results are shown in Fig. 25(b). Fig. 25(a) shows a calculated band structure of $NdO_{1-x}F_xBiS_2$. When we compare the ARPES results with the calculated band structure, the Fermi surface obtained by ARPES corresponds to the Fermi surface calculated for x=0.16. The large difference in Fermi surface between ARPES and calculation with a nominal composition of *x* is consistent with former PES results. These features could be understood by the existence of Bi defects and/or carrier distribution between the conduction BiS_2 layers and the blocking layers. To further investigate the electronic structure, ARPES on the other BiS_2 superconductors are crucial.

Another notable report on electronic states is the observation of large superconducting fluctuations revealed in STM/STS on $NdO_{1-x}F_xBiS_2$ [60]. Fig. 26 displays the STS results obtained using

$NdO_{0.5}F_{0.5}BiS_2$ single crystals. The superconducting gap is clearly observed at low temperatures. Surprisingly, the superconducting gap structure still survives up to 20 K as shown in Fig. 26(b). Here, we should note that the T_c^{zero} of this single crystal is around 4 K as shown in Fig. 26(d). However, as displayed in the inset of Fig. 26 (d), the resistivity clearly decreases with decreasing temperature below 20 K. Therefore, it was suggested that the Cooper pairs could begin to be generated below 20 K in the $NdO_{0.5}F_{0.5}BiS_2$ single crystals while the bulk superconductivity states are achieved at significantly lower temperatures below 4 K. Similar STS results were obtained for $Bi_4O_4S_3$ polycrystalline samples [66]. The existence of large superconducting fluctuations may be a common property of the BiS_2 family.

Different STM/STS results were obtained by Machida et al. using $NdO_{0.7}F_{0.3}BiS_2$ single crystals [67]. Although the bulk characteristics of the single crystals are superconducting, gap-like structure (~40 meV), insulating nature, was observed for the cleaved surface at both below and above bulk T_c as shown in Fig. 27. The different observation in these STS studies might be due to the difference in the surface states. Machida et al. measured STS on the as-cleaved surface while Liu et al. cleaned the cleaved surface by argon iron bombardment before the measurements because they also observed the insulating nature of the as-cleaved state [60]. A notable observation revealed in the as-cleaved surface of $NdO_{0.7}F_{0.3}BiS_2$ is the formation of "checkerboard stripes". This may be related to the formation of the charge-density-wave (CDW) states which has been theoretically predicted to exist in the BiS_2 layers [44,68,69]. Furthermore, if the checkerboard stripes are related to the appearance of superconductivity in the BiS_2 family, we will be able to discuss some similarities of electronic structure to the high-T_c superconductors. Although we cannot completely conclude the true properties of the electronic states of the cleaved surface of $NdO_{1-x}F_xBiS_2$ single crystals, the observations in the STM/STS measurements are quite interesting and further investigations with various BiS_2-based superconductors will

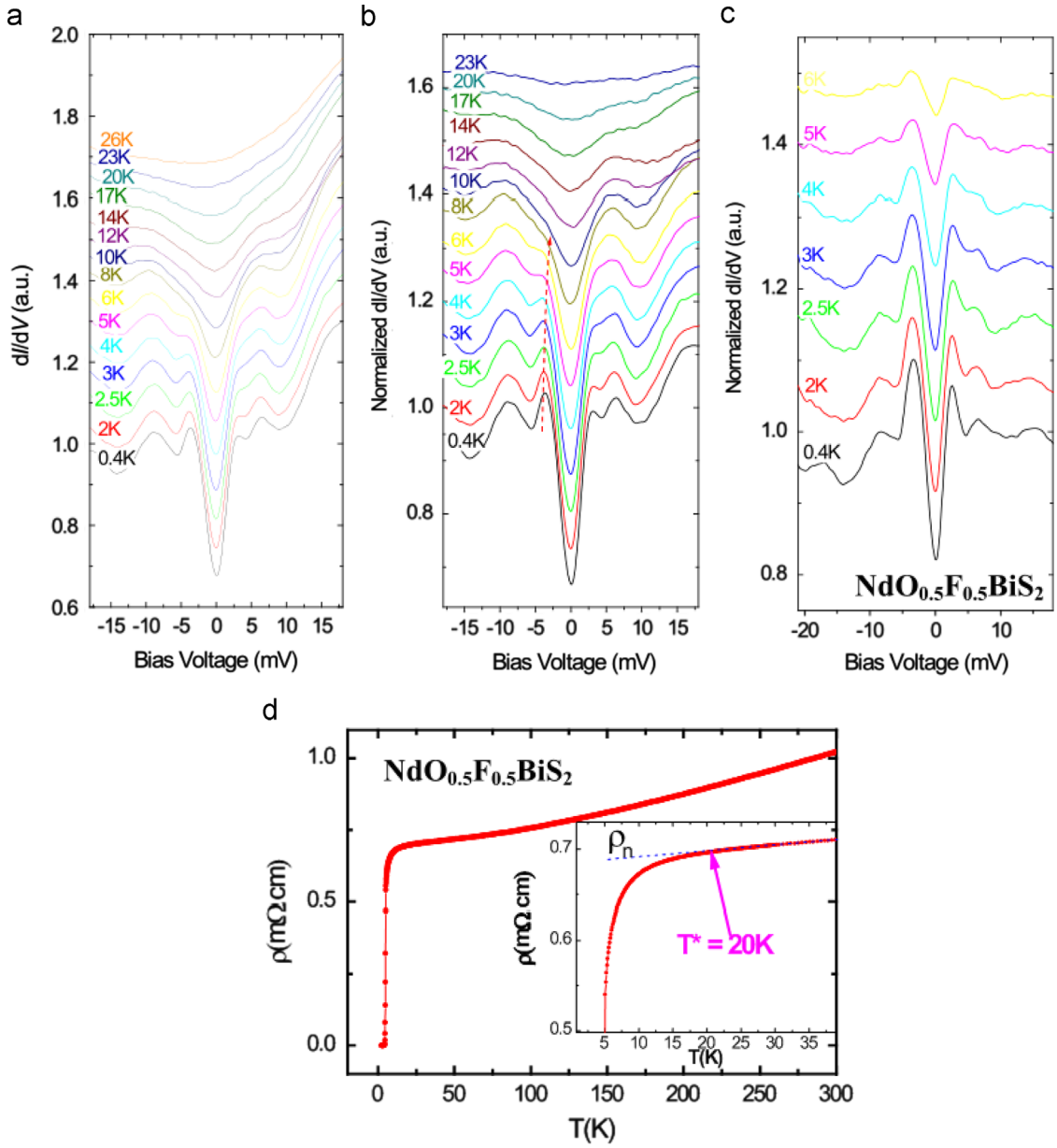

Fig. 26. (a) Evolution of the STS spectra with the temperature increased from 0.4 K to 26 K for $NdO_{0.5}F_{0.5}BiS_2$ single crystal. (b) STS spectra normalized against the normal state (at 26 K). A dashed red color line highlights the superconducting coherence peaks at around 3.5 meV. (c) STS spectra normalized against the normal state (at 8 K). (d) Temperature dependence of electrical resistivity for $NdO_{0.5}F_{0.5}BiS_2$ single crystal. The inset shows an enlarged graph around the onset of superconducting transition. [60]. (For interpretation of the references to color in this figure legend, the reader is referred to the web version of this article.)

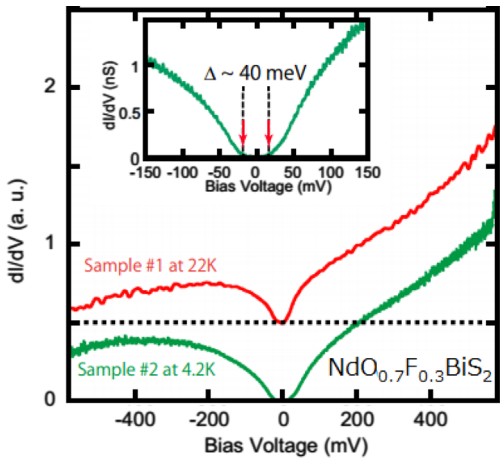

Fig. 27. Typical tunneling spectra of $NdO_{0.7}F_{0.3}BiS_2$ single crystals taken at $V_s = +500$ mV and $I_s = 1.0$ nA. Red (upper) and Green (lower) lines represents the spectra taken on the sample # 1 at 22 K and sample # 2 at 4.2 K. The red spectrum is shifted by 0.5 for clarity. The dashed line indicates the zero conductance for the red (shifted) spectrum. Inset shows the spectrum with higher energy resolution [67]. (For interpretation of the references to color in this figure legend, the reader is referred to the web version of this article.)

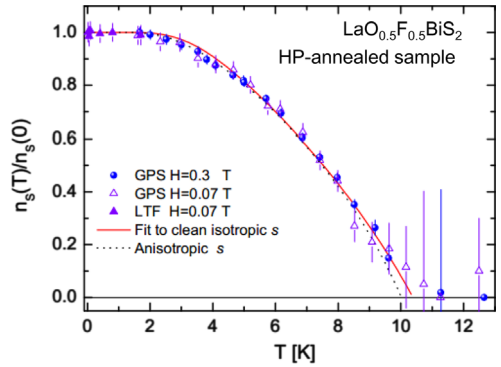

Fig. 28. Temperature dependence of the normalized superfluid density for HP-annealed $LaO_{0.5}F_{0.5}BiS_2$ measured at $\mu_0 H = 0.3$ T (full circles) and at 0.07 T (open triangles). Low-temperature ($T < 1.7$ K) data at 0.07 T are shown by solid triangles. The full and the dotted black lines represent best fits to an *s*-wave gap in the clean limit and a numerical calculation with an *s*-wave anisotropic gap [71].

give us some clues to elucidate the mechanisms of superconductivity in the BiS_2 layers.

Although the paring mechanisms of the BiS_2 family have not been clarified, two experimental studies have investigated the paring symmetry of BiS_2-based superconductors. Shruti et al. carried out measurements of magnetic penetration depth for the $Bi_4O_4S_3$ superconductor using a tunnel diode oscillator technique [70]. They concluded that $Bi_4O_4S_3$ is a conventional *s*-wave type superconductor with a fully developed gap. The zero-temperature value of the superconducting energy gap Δ_0 was 1.54 meV, which corresponds to $2\Delta_0/k_BT_c = 7.2$. The large value of $2\Delta_0/k_BT_c$ indicates the strong-coupling nature of superconductivity in $Bi_4O_4S_3$. Lamura et al. carried out μSR measurements for HP-annealed $LaO_{0.5}F_{0.5}BiS_2$ [71]. The obtained temperature dependence of normalized superfluid density for HP-annealed $LaO_{0.5}F_{0.5}BiS_2$ is shown in Fig. 28. The emergence of bulk superconducting states was revealed below 10 K. On the basis of the results, *s*-wave symmetry was suggested but, the presence of "anisotropic" superconducting gap was suggested in the measurements. In addition, some theoretical studies suggested that the pairing mechanisms of superconductivity in BiS_2-based superconductors could be explained by *d*-wave, triplet or other unconventional pairing mechanisms [47,72–74]. To clarify the pairing symmetry of BiS_2-based superconductors, further experimental and theoretical investigations are required.

7. Summary and prospects for raising T_c

In this article, the diversity of crystal structure and physical properties of the BiS_2-based layered materials have been summarized. The BiS_2-based superconductors have a crystal structure composed of an alternate stacking of BiS_2 conducting layers and blocking layers. So far, three types of blocking layer have been found as depicted in Fig. 1. The parent phase of the BiS_2 family is basically an insulator with a band gap. Electron doping into the BiS_2 conducting layers makes the BiS_2 materials metallic and induces superconductivity. One of the notable characteristics is the high sensitivity of the superconducting properties to changes in the local crystal structure and/or strain. Application of external high pressure or sample preparation under high pressure largely enhances their T_c. The highest record of T_c in the BiS_2 family is ~11 K in the HP phase of $LaO_{0.5}F_{0.5}BiS_2$. Although the mechanisms of superconductivity in BiS_2-based materials have not been clarified, we have revealed some notable properties. Firstly, the anisotropy of superconductivity in BiS_2-based materials is quite large, which is comparable to that of cuprate superconductors. Secondly, large superconducting fluctuations have been observed in $NdO_{0.5}F_{0.5}BiS_2$ single crystals and $Bi_4O_4S_3$ polycrystalline samples, suggesting that Cooper pairs could be generated at temperatures above their bulk T_c. In addition, the relation of superconductivity to charge–density–wave states should be further investigated. Furthermore, the low-carrier nature and the strong-coupling nature of superconductivity in the BiS_2-based superconductors should also be investigated in detail to elucidate the mechanisms of superconductivity in this system.

Last but not least, I would like to discuss how the T_c can be increased in the BiS_2 family. To address this issue, the typical data points of T_c for the samples whose superconducting properties were optimized are plotted in Fig. 29, namely, the T_c is the highest among the respective systems. The highest T_c is obtained for $LaO_{1-x}F_xBiS_2$. The T_c decreases with an order of $LaO_{1-x}F_xBiS_2$, $CeO_{1-x}F_xBiS_2$, $NdO_{1-x}F_xBiS_2$ and $Bi_4O_4S_3$. This tendency suggests that the T_c correlates with the blocking layer structure, particularly the T_c seems to correlate with the *a* axis length. According to this tendency, we expect a higher T_c in new BiS_2-based superconductor with a larger *a* axis length. However, the ionic radius of La is the largest among the rare earth elements which can occupy the RE site of the $REOBiS_2$ structure (Fig. 1(a)). Therefore, we must explore

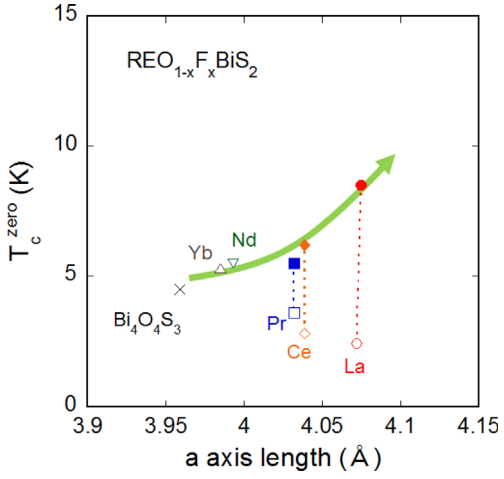

Fig. 29. Correlation between T_c and *a* axis length of typical BiS_2-based superconductors, $REO_{1-x}F_xBiS_2$ and $Bi_4O_4S_3$.

for new BiS_2-based superconductors with crystal structures of Fig. 1(b) or (c). For the $SrFBiS_2$-type, we will be able to realize a larger *a* axis length with $BaFBiS_2$. For the $Bi_4O_4(SO_4)_{1-x}Bi_2S_4$-type, we will be able to realize a larger *a* axis length by replacing the Bi site of the blocking layer with RE elements. Another strategy to realize a larger *a* axis length in the BiS_2-based materials is to discover new structures of blocking layers. Due to the structural analogy to FeAs-based superconductors, we expect new BiS_2-based materials with various types of blocking layer, for example, perovskite-type blocking layers [16,17].

Recently, new $REOBiS_2$-type superconductors containing Se have been found to be superconductive. Maziopa et al. reported that $LaO_{0.5}F_{0.5}BiSe_2$ showed superconductivity below 2.6 K [75]. Recently, Tanaka et al. observed superconductivity in $LaO_{1-x}F_x$-$BiSe_2$ single crystals [76,77]. In this material, both S sites of the $LaOBiS_2$ structure are completely substituted with Se. Although the *a* axis length is expanded as compared to $LaO_{0.5}F_{0.5}BiS_2$, the T_c is comparable. Another new superconductor is $LaO_{1-x}F_xBiSSe$ [78]. In this material, 50% of the S sites of the $LaOBiS_2$ structure is substituted with Se. A T_c of 3.8 K was observed in $LaO_{0.5}F_{0.5}BiSSe$, which is clearly higher than that of As-grown $LaO_{0.5}F_{0.5}BiS_2$. Furthermore, we can get some hints from superconductivity in doped $CsBi_4Te_6$ [79]. The T_c is 4.4 K in $Cs_{0.96}Bi_4Te_6$ single crystals. The crystal structure is composed of NaCl-type Bi_4Te_6 layers and interlayer Cs ions. Therefore, we find a structure similarity between $CsBi_4Te_6$ and BiS_2- or $BiSe_2$-based layered materials. Therefore, we will be able to explore new Bi-chalcogen superconductors by changing the blocking layers, chalcogen anions and the structure of conduction layers like Bi_4Te_6 layers (thicker superconducting layers). Although observed T_c in those materials is still lower than that (11 K) of $LaO_{0.5}F_{0.5}BiS_2$ (HP), these findings should open new physics and chemistry studies on BiS_2-related superconductors and raise T_c beyond the current highest recorded value.

References

[1] J.G. Bednorz, K.A. Müller, Z. Phys. B-Condens. Matter 64 (1986) 189.
[2] M.K. Wu, J. Ashburn, C.J. Torng, P.H. Meng, L. Gao, Z.J. Huang, U.Q. Wang, C.W. Chu, Phys. Rev. Lett. 58 (1987) 908.
[3] H. Maeda, Y. Tanaka, M. Fukutomi, T. Asano, Jpn. J. Appl. Phys. 27 (1988) L209.
[4] A. Schilling, M. Cantoni, J.D. Guo, H.R. Ott, Nature 363 (1993) 56.
[5] N. Takeshita, A. Yamamoto, A. Iyo, H. Eisaki, J. Phys. Soc. Jpn. 82 (2013) 023711.
[6] J. Nagamatsu, N. Nakagawa, T. Muranaka, Y. Zenitani, J. Akimitsu, Nature 410 (2001) 63.
[7] H. Kumakura, Jpn. J. Appl. Phys. 51 (2012) 010003.
[8] Y. Kamihara, T. Watanabe, M. Hirano, H. Hosono, J. Am. Chem. Soc. 130 (2008) 3296.
[9] X.H. Chen, T. Wu, G. Wu, R.H. Liu, H. Chen, D.F. Fang, Nature 453 (2008) 761.
[10] Z.A. Ren, W. Lu, J. Yang, W. Yi, X.L. Shen, Z.C. Li, G.C. Che, X.L. Dong, L.L. Sun, F. Zhou, Z.X. Zhao, Chin. Phys. Lett. 25 (2008) 2215.
[11] K. Ishida, Y. Nakai, H. Hosono, J. Phys. Soc. Jpn. 78 (2009) 062001.
[12] M. Rotter, M. Tegel, D. Johrendt, Phys. Rev. Lett. 101 (2008) 107006.
[13] X.C. Wang, Q.Q. Liu, Y.X. Lv, W.B. Gao, L.X. Yang, R.C. Yu, F.Y. Li, C.Q. Jin, Solid State Commun. 148 (2008) 538.
[14] F.C. Hsu, J.Y. Luo, K.W. The, T.K. Chen, T.W. Huang, P.M. Wu, Y.C. Lee, Y.L. Huang, Y.Y. Chu, D.C. Yan, M.K. Wu, Proc. Nat. Acad. Sci. 105 (2008) 14262.
[15] Y. Mizuguchi, Y. Takano, J. Phys. Soc. Jpn. 79 (2010) 102001.
[16] H. Ogino, Y. Matsumura, Y. Katsura, K. Ushiyama, H. Horii, K. Kishio, J. Shimoyama, Supercond. Sci. Technol. 22 (2009) 075008.
[17] X. Zhu, F. Han, G. Mu, P. Cheng, B. Shen, B. Zeng, H.H. Wen, Phys. Rev. B 79 (2009) 220512.
[18] M. Fujioka, S.J. Denholme, T. Ozaki, H. Okazaki, K. Deguchi, S. Demura, H. Hara, T. Watanabe, H. Takeya, T. Yamaguchi, H. Kumakura, Y. Takano, Supercond. Sci. Technol. 26 (2013) 085023.
[19] Y. Mizuguchi, H. Fujihisa, Y. Gotoh, K. Suzuki, H. Usui, K. Kuroki, S. Demura, Y. Takano, H. Izawa, O. Miura, Phys. Rev. B 86 (2012) 220510.
[20] Y. Mizuguchi, S. Demura, K. Deguchi, Y. Takano, H. Fujihisa, Y. Gotoh, H. Izawa, O. Miura, J. Phys. Soc. Jpn. 81 (2012) 114725.
[21] Y. Mizuguchi, T. Hiroi, J. Kajitani, H. Takatsu, H. Kadowaki, O. Miura, J. Phys. Soc. Jpn. 83 (2014) 053704.
[22] R.J. Cava, B. Batlogg, J.J. Krajewski, R. Farrow, L.W. Rupp Jr., A.E. White, K. Short, W.F. Peck, T. Kometani, Nature 332 (1988) 814.
[23] A.W. Sleight, J.L. Gillson, P.E. Bierstedt, Solid State Commun. 17 (1975) 27.
[24] J. Xing, S. Li, X. Ding, H. Yang, H.H. Wen, Phys. Rev. B 86 (2012) 214518.
[25] S. Demura, K. Deguchi, Y. Mizuguchi, K. Sato, R. Honjyo, A. Yamashita, T. Yamaki, H. Hara, T. Watanabe, S.J. Denholme, M. Fujioka, H. Okazaki, T. Ozaki, O. Miura, T. Yamaguchi, H. Takeya, Y. Takano, arXiv:1311.4267.
[26] R. Jha, A. Kumar, S.K. Singh, V.P.S. Awana, J. Supercond. Novel Magn. 26 (2013) 499 26 (2013).
[27] J. Kajitani, K. Deguchi, T. Hiroi, A. Omachi, S. Demura, Y. Takano, O. Miura, Y. Mizuguchi, J. Phys. Soc. Jpn. 83 (2014) 065002.
[28] S. Demura, Y. Mizuguchi, K. Deguchi, H. Okazaki, H. Hara, T. Watanabe, S. J. Denholme, M. Fujioka, T. Ozaki, H. Fujihisa, Y. Gotoh, O. Miura, T. Yamaguchi, H. Takeya, Y. Takano, J. Phys. Soc. Jpn. 82 (2013) 033708.
[29] R. Jha, A. Kumar, S.K. Singh, V.P.S. Awana, J. Appl. Phys. 113 (2013)056102 113 (2013).
[30] D. Yazici, K. Huang, B.D. White, A.H. Chang, A.J. Friedman, M.B. Maple, Philos. Mag. 93 (2012) 673.
[31] D. Yazici, K. Huang, B.D. White, I. Jeon, V.W. Burnett, A.J. Friedman, I.K. Lum, M. Nallaiyan, S. Spagna, M.B. Maple, Phys. Rev. B 87 (2013) 174512.
[32] H. Lei, K. Wang, M. Abeykoon, E.S. Bozin, C. Petrovic, Inorg. Chem. 52 (2013) 10685.
[33] X. Lin, X. Ni, B. Chen, X. Xu, X. Yang, J. Dai, Y. Li, X. Yang, Y. Luo, Q. Tao, G. Cao, Z. Xu, Phys. Rev. B 87 (2013) 020504.
[34] H. Sakai, D. Kotajima, K. Saito, H. Wadati, Y. Wakisaka, M. Mizumaki, K. Nitta, Y. Tokura, S. Ishiwata, J. Phys. Soc. Jpn. 83 (2014) 014709.
[35] F. Han, X. Zhu, G. Mu, P. Cheng, H.H. Wen, Phys. Rev. B 78 (2008) 180503.
[36] S. Matsuishi, Y. Inoue, T. Nomura, M. Hirano, H. Hosono, J. Phys. Soc. Jpn. 77 (2008) 113709.
[37] G. Wu, Y.L. Xie, H. Chen, M. Zhong, R.H. Liu, B.C. Shi, Q.J. Li, X.F. Wang, T. Wu, Y.J. Yan, J.J. Ying, X.H. Chen, J. Phys. Condens. Matter 21 (2009) 142203.
[38] H. Takatsu, Y. Mizuguchi, H. Izawa, O. Miura, H. Kadowaki, J. Phys. Soc. Jpn. 81 (2012) 125002.
[39] H. Kawaji, K.I. Hotehama, S. Yamanaka, Chem. Mater. 9 (1997) 2127.
[40] S. Yamanaka, K.I. Hotehama, H. Kawaji, Nature 392 (1998) 580.
[41] Y. Taguchi, M. Hisakabe, Y. Iwasa, Phys. Rev. Lett. 94 (2005) 217002.
[42] H. Usui, K. Suzuki, K. Kuroki, Phys. Rev. B 86 (2012) 220501.
[43] K. Suzuki, H. Usui, K. Kuroki, Phys. Procedia 45 (2013) 21.
[44] T. Yildirim, Phys. Rev. B 87 (2013) 020506.
[45] I.R. Shein, A.L. Ivanovskii, JETP Lett. 96 (2012) 769.
[46] B. Li, Z.W. Xing, G.Q. Huang, EPL 101 (2013) 47002.
[47] G. Martins, A. Moreo, E. Dagotto, Phys. Rev. B 87 (2013) 081102.
[48] C. Morice, E. Artacho, S.E. Dutton, D. Molnar, H.J. Kim, and S.S. Saxena, arXiv:1312.2615.
[49] J. Lee, M.B. Stone, A. Huq, T. Yildrim, G. Ehlers, Y. Mizuguchi, O. Miura, Y. Takano, K. Deguchi, S. Demura, S.H. Lee, Phys. Rev. B 87 (2013) 205134.
[50] K. Deguchi, Y. Mizuguchi, S. Demura, H. Hara, T. Watanabe, S.J. Denholme, M. Fujioka, H. Okazaki, T. Ozaki, H. Takeya, T. Yamaguchi, O. Miura, Y. Takano, EPL 101 (2013) 17004.
[51] R. Higashinaka, R. Miyazaki, Y. Mizuguchi, O. Miura, Y. Aoki, Low-Temperature Enhancement in the Upper Critical Field of Under doped $LaO_{1-x}F_xBiS_2$(x = 0.1-0.3), J. Phys. Soc. Jpn. 3 (2014) 75004. http://dx.doi.org/10.7566/JPSJ.83.075004.
[52] J. Kajitani, K. Deguchi, A. Omachi, T. Hiroi, Y. Takano, H. Takatsu, H. Kadowaki, O. Miura, Y. Mizuguchi, Solid State Commun. 181 (2014) 1.
[53] T. Tomita, M. Ebata, H. Soeda, H. Takahashi, H. Fujihisa, Y. Gotoh, Y. Mizuguchi, H. Izawa, O. Miura, S. Demura, K. Deguchi, Y. Takano, J. Phys. Soc. Jpn. 83 (2014) 063704.
[54] H. Kotegawa, Y. Tomita, H. Tou, H. Izawa, Y. Mizuguchi, O. Miura, S. Demura, K. Deguchi, Y. Takano, J. Phys. Soc. Jpn. 81 (2012) 103702.
[55] C.T. Wolowiec, B.D. White, I. Jeon, D. Yazici, K. Huang, M.B. Maple, J. Phys.: Condens. Matter 25 (2013) 422201.
[56] G. Kalai Selvan, M. Kanagaraj, V.P.S. Rajveer Jha S. Awana Arumugam, arXiv:1307.4877.
[57] R. Jha, B. Tiwari, V.P.S. Awana, J. Phys. Soc. Jpn. 83 (2014) 063707.
[58] M. Nagao, S. Demura, K. Deguchi, A. Miura, S. Watauchi, T. Takei, Y. Takano, N. Kumada, I. Tanaka, J. Phys. Soc. Jpn. 82 (2013) 113701.
[59] M. Nagao, A. Miura, S. Demura, K. Deguchi, S. Watauchi, T. Takei, Y. Takano, N. Kumada, I. Tanaka, Solid State Commun. 178 (2014) 33.
[60] J. Liu, D. Fang, Z. Wang, J. Xing, Z. Du, X. Zhu, H. Yang, H.H. Wen, Europhys. Lett. 106 (2014) 67002, arXiv:1310.0377.
[61] Akira Miura, Masanori Nagao, Takahiro Takei, Satoshi Watauchi, Isao Tanaka, Nobuhiro Kumada, J. Solid State Chem. 212 (2014) 213.
[62] S.L. Bud'ko, V.G. Kogan, P.C. Canfield, Phys. Rev. B 64 (2001) 180506.
[63] Y. Mizuguchi, A. Miyake, K. Akiba, M. Tokunaga, J. Kajitani, O. Miura, Phys. Rev. B 89 (2014) 174515.
[64] S. Nagira, J. Sonoyama, T. Wakita, M. Sunagawa, Y. Izumi, T. Muro, H. Kumigashira, M. Oshima, K. Deguchi, H. Okazaki, Y. Takano, O. Miura, Y. Mizuguchi, K. Suzuki, H. Usui, K. Kuroki, K. Okada, Y. Muraoka, T. Yokoya, J. Phys. Soc. Jpn. 83 (2014) 033703.
[65] Z.R. Ye, H.F. Yang, D.W. Shen, J. Jiang, X.H. Niu, D.L. Feng, Y.P. Du, X.G. Wan, J. Z. Liu, X.Y. Zhu, H.H. Wen, M.H. Jiang, Phys. Rev. B 90 (2014) 045116, arXiv:1402.2860.
[66] S. Li, H. Yang, J. Tao, X. Ding, H.H. Wen, Sci China: Phys. Mech. Astron. 56 (2013) 2019.
[67] T. Machida, Y. Fujisawa, M. Nagao, S. Demura, K. Deguchi, Y. Mizuguchi, Y. Takano, H. Sakata, arXiv:1403.6110.
[68] X. Wan, H.C. Ding, S.Y. Savrasov, C.G. Duan, Phys. Rev. B 87 (2013) 115124.
[69] J. Xing, S. Li, X. Ding, H. Yang, H.H. Wen, Phys. Rev. B 86 (2012) 214518.
[70] P. Srivastava Shruti, S. Patnaik, J. Phys.: Condens. Matter 25 (2013) 312202.

[71] G. Lamura, T. Shiroka, P. Bonfa, S. Sanna, R. De Renzi, C. Baines, H. Luetkens, J. Kajitani, Y. Mizuguchi, O. Miura, K. Deguchi, S. Demura, Y. Takano, M. Putti, Phys. Rev. B 88 (2013) 180509.
[72] Y. Liang, X. Wu, W.F. Tsai, J. Hu, Front. Phys. 9 (2014) 194.
[73] Y. Yang, W.S. Wang, Y.Y. Xiang, Z.Z. Li, Q.H. Wang, Phys. Rev. B 88 (2013) 094519.
[74] X. Wu, J. Yuan, Y. Liang, H. Fan, J. Hu, arXiv:1403.5949.
[75] A.K. Maziopa, Z. Guguchia, E. Pomjakushina, V. Pomjakushin, R. Khasanov, H. Luetkens, P.K. Biswas, A. Amato, H. Keller, K. Conder, J. Phys.: Condens. Matter 26 (2014) 215702.
[76] M. Tanaka, M. Nagao, Y. Matsushita, M. Fujioka, S.J. Denholme, T. Yamaguchi, H. Takeya, Y. Takano, J. Solid State Chem. 219 (2014) 168–172, arXiv:1406.0734.
[77] M. Nagao, M. Tanaka, S. Watauchi, I. Tanaka, Y. Takano, arXiv:1406.0921.
[78] X.C. Wang, D.Y. Chen, Q. Guo, J. Yu, B.B. Ruan, Q.G. Mu, G.F. Chen, Z.A. Ren, arXiv:1404.7562.
[79] C.D. Malliakas, D.Y. Chung, H. Claus, M.G. Kanatzidis, J. Am. Chem. Soc. 135 (2013) 14540.